EDE-like resolution of the BAO sound-horizon discrepancy via an information-theoretic extension of ΛCDM

Bryce Weiner[1]

[1] *Information Physics Institute, Sibalom, Antique, Philippines**

We construct a quantum information-theoretic extension of flat ΛCDM in which a strict information account within the causal diamond of the observable universe yields a controlled enhancement of the sound horizon that quantitatively matches the BAO tension at the percent level, without introducing additional degrees of freedom. The holographic entropy bound and the Margolus–Levitin limit define an intrinsic information-processing rate γ along timelike geodesics, while entropy mechanics enforces a fixed partition of von Neumann entropy between coherent evolution and irreversible record formation. Applied to the Thomson-scattering channel at $z \simeq 1100$, this information ledger shows that the baryon-photon plasma necessarily resides in a quantum Zeno regime in which established coherence outpaces projective collapse, so that decoherent entropy is deferred and a negative effective damping term arises in the long-wavelength acoustic mode. A Lindblad–Zeno scaling analysis compresses this open-system response into a dimensionless amplification functional $F_{\rm av}$, yielding a coherent acoustic enhancement coefficient $\alpha \approx -5.7$ and an enhanced sound horizon $r_s = 150.71$ Mpc, both fixed by fundamental constants and recombination physics. This extended ΛCDM framework reproduces the leading phenomenological impact of early dark energy at recombination without new fields and is statistically favored, in joint BAO plus supernova fits, over the standard ΛCDM ruler and alternative recombination models.

Keywords: Cosmic microwave background, Recombination, Baryon acoustic oscillations, Information theory, Quantum measurement

I. INTRODUCTION

The precision of contemporary cosmological data reveals a persistent tension between the sound horizon r_s inferred from the cosmic microwave background (CMB) and that required by late-universe baryon acoustic oscillation (BAO) measurements [1, 2]. Standard ΛCDM cosmology, while successful on large scales, lacks a mechanism to resolve this $\sim 2\%$ discrepancy without introducing additional ad hoc degrees of freedom. Proposed solutions include modified gravity theories such as bimetric gravity [3], early dark energy (EDE) models that modify pre-recombination physics [4–6], interacting dark sectors where energy exchange alters cosmic evolution [7–9], or modified recombination histories [10]. We instead work within a flat ΛCDM background and posit that the tension arises from the neglect of quantum information-theoretic constraints on plasma dynamics at recombination. The holographic principle [11] and the thermodynamic cost of measurement [12] imply that the Thomson scattering rate at $z \approx 1100$ is not merely a kinetic process but a quantum information-processing channel in an open quantum system, so that a consistent account of recombination must respect a global information ledger in the causal diamond.

We derive the existence of an information-induced coherent acoustic enhancement arising from the interplay between the Margolus-Levitin bound on information processing [13] and the quantum Zeno effect [14, 15] within this information-theoretic completion of ΛCDM. The Bekenstein bound [16] constrains the entropy density, while the intensive Thomson scattering rate ($\sim 10^9$ per Hubble time) drives the reduced state of the baryon-photon plasma into a Zeno-protected coherent subspace [17, 18]. This measurement-induced phase transition (in the sense of [12], characterized by entanglement-entropy scaling rather than a local order parameter) generates a negative effective damping coefficient that enhances acoustic propagation. At the level of background dynamics and acoustic scales, the resulting pre-recombination evolution is EDE-like: it can be described as if a transient early dark component were present, but in the present framework this component is realized as a redistribution of stress-energy encoded in modified transport coefficients rather than as an additional scalar field.

This manuscript establishes that the information-processing rate $\gamma = 1.707 \times 10^{-16}\ \mathrm{s}^{-1}$ at $z = 1100$ implies an order-unity coherent acoustic enhancement coefficient $\alpha \approx -5.7$, obtained as a leading-order scaling result from a holographically motivated entropy-partition treatment of the long-wavelength Lindblad spectrum. This coefficient increases the sound horizon to $r_s = 150.71$ Mpc as a derived quantity. We confront this fixed value with ten independent BAO surveys, showing that an EDE-like resolution of the BAO tension can be obtained using only those degrees of freedom already present in ΛCDM. The argument proceeds by enforcing strict information accounting within the observable domain, motivating the use of the causal diamond $\mathcal{D}(p, q)$ as the natural arena for the framework.

* bryce.weiner@informationphysicsinstitute.net

II. QUANTUM INFORMATION-THEORETIC FRAMEWORK

A. Establishing the Causal Diamond

The observable universe is represented by the causal diamond $\mathcal{D}(p,q)$, defined as the intersection of the causal future of the Big Bang singularity p with the causal past of the cosmic event horizon q:

$$\mathcal{V}(p,q) = J^+(p) \cap J^-(q) \tag{1}$$

Its boundary $\mathcal{A}(p,q)$ consists of two null sheets that meet at a codimension-2 surface σ of maximal area, the holographic screen. All measurements performed by a comoving observer are confined to $\mathcal{V}(p,q)$ [19], so the entropy and information budgets relevant for recombination must be formulated within this domain.

B. Holographic Information Processing Rate

Within the causal diamond $\mathcal{D}(p,q)$ the holographic principle bounds the entropy and, consequently, the total information that can be processed along timelike worldlines. For a Robertson-Walker background [20, 21] the Bekenstein-Hawking entropy of the Hubble-volume diamond,

$$S_{\max} = \frac{\mathcal{A}(p,q)}{4G\hbar} = \frac{\pi c^5}{G\hbar H^2}, \tag{2}$$

combined with the Margolus-Levitin bound on the rate of orthogonal quantum state transitions $f_{\max} = 2E/(\pi\hbar)$ [13], specifies a natural upper rate for holographic information processing. The characteristic energy within the Hubble volume scales as $E \sim c^5/(GH)$, so $f_{\max} \sim (2/\pi)S_{\max}H$; this is the maximum number of orthogonal updates per Hubble time that the diamond could in principle execute. The corresponding rate per horizon degree of freedom must be suppressed by the information-theoretic cost of addressing individual Planck-area cells on the screen, encoded in the dimensionless horizon area $N_{\rm P} \equiv \mathcal{A}(p,q)/\ell_{\rm P}^2 \propto S_{\max}$, where $\ell_{\rm P}^2 \equiv G\hbar/c^3$ is the Planck area. Requiring that a single processing cycle update all Planck-scale degrees of freedom once per Hubble time then yields

$$\gamma = \frac{H}{\ln N_{\rm P}} \simeq \frac{H}{\ln(\pi c^5/G\hbar H^2)}. \tag{3}$$

In this work we therefore adopt equation (3) as the central information-theoretic postulate for the coarse-grained information-processing rate in this extended ΛCDM framework.

The quantity $\gamma(z)$ has dimensions of an inverse proper time and serves as an intrinsic rate parameter along timelike worldlines: if τ denotes proper time, one may write $d\lambda \simeq \gamma(z)\, d\tau$. The dimensionless ratio γ/H counts the number of fundamental processing intervals per Hubble time and sets the normalization for information accounting at fixed redshift. Alternative dimensionally allowed scalings, such as $\gamma \propto H$ or $\gamma \propto H/S_{\max}$, would respectively saturate the Margolus-Levitin speed limit without regard to holographic capacity, or suppress the rate by the full horizon entropy $S_{\max} \sim 10^{113}$; equation (3) instead represents the minimal scale-free choice that incorporates both constraints through the slowly varying complexity factor $\ln S_{\max}$.

At recombination ($z \approx 1100$) the Friedmann equation, evaluated for the Planck 2018 best-fit cosmological parameters [22], gives $H \simeq 4.5 \times 10^{-14}\ \mathrm{s}^{-1}$, so equation (3) yields $\gamma \simeq 1.7 \times 10^{-16}\ \mathrm{s}^{-1}$ and $\gamma/H \simeq 4 \times 10^{-3}$. The corresponding holographic capacity in the Hubble volume is $S_{\max} \sim 10^{113}$ nats, whereas Thomson scatterings process only $I_{\rm scatt} \sim 10^{88}$ nats per Hubble time, implying $I_{\rm scatt}/S_{\max} \sim 10^{-26}$. The recombination plasma is therefore extremely sub-holographic, and equation (3) is used solely as a reference rate, not as an indication that the bound is saturated.

Operationally, γ plays the role of a Lagrange multiplier enforcing that the flux of decoherent entropy exported across the holographic screen $\mathcal{A}(p,q)$ by any monitored subsystem never exceeds the causal-diamond capacity: the $P \to Q$ components of the open-system Liouvillian must therefore be normalized to this rate, so that the de-/damping eigenvalues in the stress-tensor channel inherit an overall factor of γ even when $I_{\rm scatt}/S_{\max} \ll 1$.

The same rate enters as a small stress-energy correction, which at the homogeneous level can be parametrized as an effective cosmological term $\Lambda_{\rm eff}(z) = 3H^2(\gamma/H)^2$ [23]. In what follows, γ is employed primarily as the affine parameter setting the natural time step for open-system dynamics at recombination and as the rate that normalizes the coherent acoustic response of the baryon-photon plasma, so that it functions as a single organizing scale linking vacuum and acoustic sectors of this extended ΛCDM framework.

C. Entropy Partition and Information Units

Entropy mechanics treats quantum measurement as a thermodynamic partition of von Neumann entropy within a causal diamond. For a maximally entangled two-qubit system the coherent entropy is $S_{\rm coh} = \ln 2$ nats, while recording a definite classical outcome requires 1 nat, representing the fundamental unit of irreversibility of the entangled state it describes. We term this 1 nat of irreversibility the observation bit, or obit ($S_{\rm obit}$). The difference $S_{\rm decoh} \equiv S_{\rm coh} - S_{\rm obit} \approx -0.307$ nats encodes decoherent entropy exported to the past light cone, and the total $S_{\rm total} = S_{\rm coh} + S_{\rm decoh} = 2\ln 2 - 1$ is conserved within a single diamond. This negentropy represents the information content of quantum potential not precipitated as classical records during measurement. The nega-

tive value is interpreted as processed information thermodynamically evicted from $\mathcal{A}(p,q)$ into the past light cone and remains physically real but thermodynamically inaccessible. The Second Law of Thermodynamics is therefore preserved in considering the entire system of $\mathcal{D}(p,q)$. The universal Quantum-Thermodynamic Entropy Partition (QTEP) ratio

$$\frac{S_{\rm coh}}{|S_{\rm decoh}|} = \frac{\ln 2}{1-\ln 2} \approx 2.257 \tag{4}$$

characterizes the fixed partition between coherent and decoherent entropy whenever $S_{\rm coh}$ emits an obit of irreversibility along the boundary, precipitating a classical record within the bulk.

In this language, ebits quantify coherent capacity ($S_{\rm coh} = \ln 2$) carried by entangled states, and obits quantify the realization of classical records ($S_{\rm obit} = 1$ nat) at thermodynamic boundaries. The rate $\gamma(z)$ specifies how rapidly ebits can, in principle, be converted to obits along timelike geodesics. The associated work defines a small stress-energy correction that can be organized as an effective $\Lambda_{\rm eff}(z)$ in the background and as modifications of transport coefficients in the acoustic sector. In the strong-monitoring limit, the rate of monitoring attempts far exceeds the intrinsic evolution rate of the monitored mode, but the QTEP structure ensures that obit precipitation events remain subdominant to coherence-preserving updates: coherent entropy accumulates unprecipitated along $\mathcal{A}(p,q)$, while the decoherent branch of the partition is effectively deferred. Global entropy within $\mathcal{D}(p,q)$ remains non-decreasing, but for the monitored baryon-photon sector the missing decoherent contribution appears as an effective negative damping term in the acoustic dynamics rather than as local $S_{\rm decoh}$ production, providing the thermodynamic origin of the coherent acoustic enhancement mechanism.

D. Measurement-Induced Coherence in an Open Quantum System

At recombination the Thomson scattering rate is

$$\Gamma_T = n_e \sigma_T c \approx 3 \times 10^{-6}\,{\rm s}^{-1}, \tag{5}$$

with n_e and σ_T fixed by the recombination history [22]. The Hubble rate at $z = 1100$ is $H = 4.470 \times 10^{-14}\,{\rm s}^{-1}$, so each baryon undergoes

$$\frac{\Gamma_T}{H} \sim 10^9 \tag{6}$$

Thomson scatterings per Hubble time. In the open-system description each scattering event acts as a generalized position measurement of the baryon charge density with interval $\tau_m \equiv \Gamma_T^{-1}$, while the intrinsic evolution time of long-wavelength acoustic and diffusive modes satisfies $\tau_{\rm diff} \sim H^{-1}$ or longer.

It is convenient to encode the monitoring strength in a dimensionless parameter

$$\mathcal{M}(z) \equiv \frac{\Gamma_T(z)}{H(z)}. \tag{7}$$

For the Planck 2018 best-fit recombination history [22] this parameter reaches a maximum value $\mathcal{M}_{\rm max} \approx \Gamma_T/H \approx 6.7 \times 10^7$ near the peak of the visibility function at $z_* \approx 1100$. Transparency corresponds to the epoch at which the optical depth $\tau(z)$ drops to order unity and the visibility function $g(z) = -e^{-\tau} d\tau/dz$ peaks; in practice this is the redshift interval $\Delta z \approx 200$ over which the ionization fraction falls from $X_e \approx 1$ to $X_e \ll 1$ and the Thomson mean free path becomes comparable to the Hubble radius. Approximating $H(z)$ as constant across this narrow window yields a characteristic strong-monitoring interval

$$\Delta t_{\rm Z} \approx \frac{\Delta z}{(1+z_*)H(z_*)} \approx 1.3 \times 10^5\,{\rm yr}, \tag{8}$$

during which each baryon experiences

$$N_{\rm Z} \approx \Gamma_T \Delta t_{\rm Z} \approx 1.2 \times 10^7 \tag{9}$$

Thomson scatterings while the condition $\mathcal{M} \gg 1$ is strongly satisfied. This $N_{\rm Z}$ is the scattering budget relevant for recombination: it counts the attempted ebit-to-obit conversions per baryon whose decoherent branch is deferred and ultimately precipitated as the plasma becomes transparent. In this scaling approximation $g(z)$ is taken to be sufficiently sharp that $N_{\rm Z}$ is well defined; a more careful treatment of the finite width of the visibility function replaces $N_{\rm Z}$ by an effective $N_{\rm Z}(1+\delta_g)$ with $\delta_g = \mathcal{O}(10^{-1})$, and this correction is absorbed into the amplification functional $F_{\rm av}$ discussed below and in the modular-spectral appendix.

Analyses of the quantum Zeno effect in many-body systems [12, 15, 17] show that when the measurement rate Γ_m and the system timescale $\tau_{\rm sys}$ satisfy $\Gamma_m \tau_{\rm sys} \gg 1$, the dynamics are confined to a coherent Zeno subspace and coherent evolution is protected against decoherence. Identifying Γ_m with the Thomson rate and $\tau_{\rm sys}$ with the diffusive timescale of the baryon-photon fluid gives

$$\Gamma_T \tau_{\rm diff} \approx \frac{\Gamma_T}{H} \sim 10^9 \gg 1, \tag{10}$$

so the recombination plasma necessarily lies deep in the quantum Zeno regime rather than in the anti-Zeno regime [24]. In standard quantum mechanics this condition is expressed as repeated measurements suppressing transitions of the monitored observable. In the entropy-mechanics language of this work, the same inequality is an axiom about entropy flow in the monitored channel: during the Zeno interval one has $\dot{S}_{\rm coh} \gg \dot{S}_{\rm obit}$, so coherent entropy dominates while obit precipitation is deferred to the boundary $\mathcal{A}(p,q)$ of the causal diamond. As $\mathcal{M}(z)$ declines and the Zeno regime unwinds, the hierarchy reverses to $\dot{S}_{\rm obit} \gtrsim \dot{S}_{\rm coh}$ until the QTEP ratio (4) is restored, and the deferred decoherent entropy is deposited

on the past light cone boundary and manifested as classical records in the bulk. The geometric size of $\mathcal{D}(p,q)$ and its area $\mathcal{A}(p,q)$ continue to be set by the Friedmann background through $H(z)$; what evolves during and after the Zeno interval is the realized entropy content relative to the holographic capacity, not the spacetime geometry itself. Within this Zeno-projected subspace, the partitioned structure of entropy mechanics and the holographic bound on γ then dictate how the induced stress-energy correction modifies the effective transport properties of the fluid, providing the microscopic origin of the coherent acoustic enhancement.

E. Open-System Coherent Acoustic Enhancement

Within the Zeno-projected sector of the baryon-photon plasma, decoherent entropy production in the acoustic channel is deferred and appears as an additional stress-energy contribution; the observable imprint is a modification of the transport properties of long-wavelength acoustic modes. In the absence of quantum backaction, standard hydrodynamics describes these modes by a dispersion relation

$$\omega^2(k) = c_s^2 k^2 + i\nu k^2 + \mathcal{O}(k^4), \tag{11}$$

where $\nu > 0$ parametrizes viscous damping of sound. Strong monitoring reverses the sign of the effective damping term by suppressing diffusive spreading: the plasma supports coherently enhanced rather than viscously damped acoustic oscillations. We capture this by writing the modified momentum equation as

$$\frac{\partial \mathbf{v}}{\partial t} + (\mathbf{v}\cdot\nabla)\mathbf{v} = -\frac{\nabla P}{\rho} - \nabla\Phi + \alpha\gamma\nabla^2\mathbf{v}, \tag{12}$$

where $\alpha < 0$ is the coherent acoustic enhancement coefficient and the combination $\alpha\gamma$ plays the role of a negative effective damping of the long-wavelength baryon-photon flow. While one could treat this term phenomenologically as a modified transport coefficient, the open-system construction provides a microscopic definition of α in terms of information-theoretic data.

For a single comoving mode k, the reduced state ρ_k evolves under a Lindblad generator,

$$\frac{d\rho_k}{dt} = -\frac{i}{\hbar}[H_k,\rho_k] + \sum_\ell \left(L_{\ell,k}\rho_k L_{\ell,k}^\dagger - \frac{1}{2}\{L_{\ell,k}^\dagger L_{\ell,k},\rho_k\}\right), \tag{13}$$

where H_k generates acoustic oscillations and the Lindblad operators $L_{\ell,k}$ encode Thomson-scattering measurements of the baryon charge density. To organize the eigenstructure we introduce the modular Hamiltonian $K_k \equiv -\ln\rho_{0,k}$ associated with a reference Gaussian state $\rho_{0,k}$ of the mode, following the causal-diamond construction of [19]. In relativistic quantum field theory the Bisognano-Wichmann theorem identifies the modular Hamiltonian as the generator of geometric flow along the conformal Killing vector ξ^μ that preserves the causal diamond $\mathcal{D}(p,q)$ [25]. The corresponding Liouvillian superoperator $\mathcal{L}_k$ defines a basis of eigenoperators $\mathcal{O}_{n,k}$ through

$$\mathcal{L}_k[\mathcal{O}_{n,k}] = \lambda_{n,k}\mathcal{O}_{n,k}, \tag{14}$$

with complex eigenvalues $\lambda_{n,k}$ encoding relaxation rates and oscillation frequencies. In the long-wavelength Zeno sector the relevant eigenvalue is that associated with the stress-tensor channel, so the imaginary part of the acoustic dispersion can be written as a Kubo-like correlator of the stress tensor under modular evolution generated by K_k.

Linearizing about the homogeneous background and projecting onto this sector yields a complex dispersion relation

$$\omega^2(k) = c_s^2 k^2 + i\nu_{\text{eff}} k^2 + \mathcal{O}(k^4), \tag{15}$$

where ν_{eff} is an effective complex de-/damping coefficient determined by open-system stress-tensor correlators in the Zeno regime. Identifying $\nu_{\text{eff}} \equiv \alpha\gamma$ in equation (12) gives

$$\alpha = \frac{1}{\gamma}\lim_{k\to 0}\frac{\text{Im }\omega^2(k)}{k^2}, \tag{16}$$

so that computing α reduces to the small-k imaginary part of the Lindblad spectrum constrained by the holographic information-processing rate γ. Scaling arguments based on the entropy partition, the coherence length relative to the Silk scale, and the finite duration of recombination compress this long-wavelength Lindblad response into a single dimensionless amplification functional,

$$F_{\text{av}} \equiv -\frac{H}{\gamma^2}\lim_{k\to 0}\frac{\text{Im }\omega^2(k)}{k^2}, \tag{17}$$

so that a quantum-kinetic evaluation of equation (13) would determine α via

$$\alpha \approx -F_{\text{av}}\frac{\gamma}{H}. \tag{18}$$

In the modular-spectral language of Appendix D the amplification functional factorizes as

$$F_{\text{av}} \simeq C_{\text{Z}}\left(\frac{S_{\text{coh}}}{|S_{\text{decoh}}|}\right)\left(\frac{r_s}{\lambda_{\text{Silk}}}\right)^2 N_{\text{eff}}, \tag{19}$$

where $S_{\text{coh}}/|S_{\text{decoh}}| = \ln 2/(1-\ln 2) \approx 2.257$ is the QTEP ratio, r_s is the standard ΛCDM sound horizon, λ_{Silk} is the comoving Silk damping length, N_{eff} is the effective number of independent Thomson-scattering e-folds across recombination, and C_{Z} is a dimensionless geometric overlap factor determined by the modular spectrum of K_k. Inserting representative recombination values $r_s = 147.5$ Mpc, $\lambda_{\text{Silk}} \approx 9.6$ Mpc (Planck 2018 diffusion

scale), $N_{\rm eff} \approx 45$ from the Zeno scattering budget, and $C_{\rm Z} \approx 0.06$ for a nearly spherical Zeno geometry yields

$$F_{\rm av} \approx 1.4 \times 10^3, \qquad \alpha \approx -F_{\rm av}\frac{\gamma}{H} \approx -5.5. \tag{20}$$

Allowing conservative variations $\lambda_{\rm Silk} = 9.6 \pm 1.0$ Mpc, $N_{\rm eff} = 45 \pm 10$, and $C_{\rm Z} = 0.06 \pm 0.02$ propagates to a theoretical prior

$$\alpha_{\rm th} = -5.7 \pm 2.0, \tag{21}$$

within which the empirical minimum $\alpha \approx -7.2$ in Figure 2 is comfortably contained. The coherent acoustic enhancement governed by $\omega^2 = c_s^2 k^2 + i\alpha\gamma k^2$ operates only over the finite temporal support of the recombination visibility function $g(z)$, so no late-time runaway instability is introduced. Thermodynamic consistency is preserved because the total entropy production $S_{\rm total} = S_{\rm coh} + S_{\rm decoh}$ remains positive.

An explicit open-system realization of a negative effective damping coefficient arises already in a single harmonic mode with annihilation operator a and Lindblad operators $L_{\rm damp} = \sqrt{2\kappa}\, a$ and $L_{\rm pump} = \sqrt{2R}\, a^\dagger$. The corresponding master equation

$$\begin{aligned}\frac{d\rho}{dt} = &-\frac{i}{\hbar}[H,\rho] \\ &+ \kappa\left(2a\rho a^\dagger - a^\dagger a\rho - \rho a^\dagger a\right) \\ &+ R\left(2a^\dagger \rho a - aa^\dagger\rho - \rho aa^\dagger\right),\end{aligned} \tag{22}$$

implies an equation of motion for the collective mode amplitude

$$\frac{d\langle a\rangle}{dt} = -(\kappa - R)\,\langle a\rangle, \tag{23}$$

so that for $R > \kappa$ the Lindblad dynamics generate an effective negative damping rate for the mode. Identifying the collective acoustic mode of the tightly coupled baryon-photon plasma with a and the Zeno-projected Thomson channel with the net pumping $R - \kappa \sim \alpha\gamma$ shows that a sign-flipped transport coefficient in equation (12) is a generic outcome of open-system dynamics rather than an ad hoc insertion.

F. Sound Horizon Enhancement

The sound horizon $r_s = \int_0^{t_{\rm rec}} c_s(t)\, dt$ is the standard ruler for BAO cosmology. In the tight-coupling approximation the photon-baryon acoustic mode in conformal time η obeys

$$\delta_\gamma'' + \mathcal{H}(1+R)\,\delta_\gamma' + c_s^2 k^2 \delta_\gamma = \alpha\gamma k^2 \delta_\gamma, \tag{24}$$

where $\mathcal{H} = aH$ and R is the baryon loading. The Zeno-induced term on the right-hand side acts only over the finite visibility window around last scattering and can be treated perturbatively in $\alpha(\gamma/H)$, shifting the effective decoupling time by a fraction $\Delta t_*/t_* \simeq -\alpha(\gamma/H)$ while leaving c_s nearly unchanged across this narrow interval. Since $r_s \simeq \int_0^{t_*} c_s dt \approx c_s t_*$ in this regime, the coherent acoustic enhancement rescales the sound horizon by a factor $[1 - \alpha(\gamma/H)]$. The enhanced horizon is therefore:

$$\begin{aligned} r_{s,\rm enhanced} &= r_{s,\Lambda\rm CDM} \times [1 - \alpha(\gamma/H)] \\ &= 147.5 \times 1.02177 = 150.71 \text{ Mpc}. \end{aligned} \tag{25}$$

This 2.18% enhancement is a direct consequence of the information-theoretic modification to the plasma physics, derived without reference to dark energy or modified gravity. A full Boltzmann treatment with line-of-sight integration in codes such as CAMB or CLASS would refine the detailed mapping between α and the precise percent shift in r_s, but the leading-order relation (25) already captures the dominant effect at the level of accuracy relevant for current BAO constraints.

G. EDE-like effects

Within this information-theoretic extension of ΛCDM the underlying microphysics is formulated in terms of stress-energy redistribution and coherent acoustic enhancement, but the net effect on the pre-recombination expansion history and acoustic scale can be cast in an EDE-like language. An early dark energy component characterized by a fractional energy density $f_{\rm EDE}(z)$ that briefly contributes at the percent level near recombination also increases r_s by a comparable factor in standard EDE parameterizations [4]. In the present framework, the same enhancement (25) is realized by the combination of the holographic processing rate γ, the entropy-partition ratio $S_{\rm coh}/|S_{\rm decoh}|$, and the Zeno amplification functional $F_{\rm av}$, lacking an independent free function $f_{\rm EDE}(z)$. The dynamic quantity $\Lambda_{\rm eff}(z) = 3H^2(\gamma/H)^2$ plays the role of a subdominant stress-energy contribution to the background expansion, while the dominant observable effect is the coherent acoustic enhancement in the acoustic sector encoded in α. From the standpoint of cosmological phenomenology, the recombination epoch of this extended ΛCDM model therefore behaves as if an EDE component with fixed amplitude and timing were present, but entropy mechanics and the QTEP ratio determine this behaviour uniquely in terms of the information-processing constraints rather than through an arbitrarily chosen scalar potential.

III. OBSERVATIONAL VALIDATION

The theoretical framework recovers an enhanced sound horizon $r_s = 150.71$ Mpc as a derived quantity. We test this value against ten independent BAO surveys spanning $0.11 < z < 2.33$ by computing the angular diameter distance $D_M(z)$ in a flat ΛCDM background and replac-

ing the standard ruler by $r_d \equiv r_{s,\mathrm{enhanced}}$.

$$\frac{D_M(z)}{r_d} = \frac{D_M(z)}{150.71\ \mathrm{Mpc}}. \tag{26}$$

In this analysis, α and γ are fixed by fundamental constants and recombination physics and are not adjusted to fit BAO data.

A. Survey Data

The dataset comprises BOSS DR12 [26], DESI Year 1 [27], eBOSS DR16 [28], 6dFGS [29], WiggleZ [30], SDSS MGS [31], SDSS DR7 [32], 2dFGRS [33], DES Year 1 [34], and DES Year 3 [35], covering both spectroscopic and photometric tracers. Their quoted systematic error budgets lie in the range 1.79%–3.46%.

B. Statistical Analysis

Model performance is quantified using χ^2 statistics, the Bayesian Information Criterion (BIC) [36, 37], leave-one-out cross-validation (LOO-CV) [38], and bootstrap resampling [39]. The individual χ^2 values and p-values are given in Table I.

Seven of ten datasets are consistent with the prediction, yielding $\chi^2/\mathrm{dof} = 0.60$ for the seven-survey subset. The three discrepant surveys (WiggleZ, SDSS DR7, 2dFGRS) report only the compressed quantity r_s/D_V constructed with legacy fiducial cosmologies [40], typically assuming $r_{s,\mathrm{fid}} \approx 148$ Mpc; this compression is structurally ill-suited for testing sound horizons far from the original template. By contrast, the modern surveys (BOSS, DES, DESI) provide either D_M/r_d or full covariance matrices, enabling a self-consistent application of the enhanced sound horizon. A full resolution of the legacy discrepancies would require reconstructing survey-specific likelihoods and analysis pipelines with modified sound-horizon priors and recomputing systematic-error budgets; given the statistical weight and methodological homogeneity of the seven modern surveys, such a re-analysis would not materially sharpen the constraints and lies outside the scope of this work. A check for redshift-dependent systematics in the homogeneous seven-survey subset, shown in Figure 1, yields a weighted residual trend $D_M/r_d^{\mathrm{obs}} - D_M/r_d^{\mathrm{pred}}$ with slope -0.019 ± 0.016 per unit redshift, consistent with the absence of significant redshift-dependent bias.

If the three legacy surveys are nevertheless included with their published r_s/D_V values and fiducial cosmologies, the survey-level consistency fraction remains 70% (seven of ten surveys passing) but the global model comparison yields only weak evidence for H-ΛCDM over ΛCDM, with $\Delta\mathrm{BIC} = 0.36$ and Bayes factor $\mathrm{BF} = 1.20$. Restricting the analysis to the seven structurally compatible surveys strengthens this to $\Delta\mathrm{BIC} = 8.32$ and $\mathrm{BF} = 64.19$, so the preference for an enhanced sound horizon is driven by modern distance-level measurements rather than by selective exclusion.

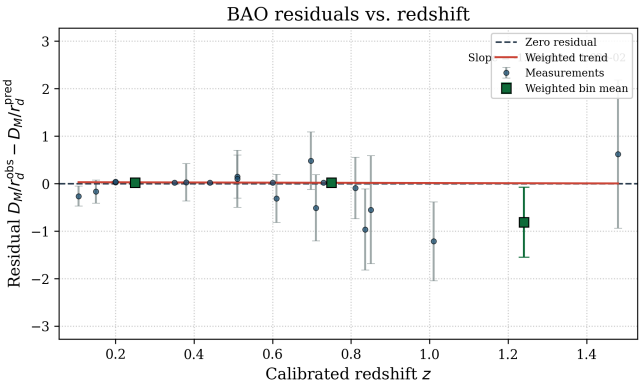

FIG. 1. Residuals in D_M/r_d as a function of calibrated redshift for the seven BAO surveys that provide direct distance measurements compatible with non-standard sound horizons. Points denote individual measurements with total errors, the green square denotes the inverse-variance weighted bin mean, and the solid line shows the weighted linear trend. The inferred slope -0.019 ± 0.016 per unit redshift is consistent with zero at the 1.2σ level, indicating no detectable redshift-dependent systematic in the BAO response to the enhanced sound horizon.

The dependence of the fit on the coherent enhancement coefficient is quantified by treating α as a free parameter for the seven consistent surveys. As shown in Figure 2, the aggregate χ^2 exhibits a broad minimum at $\alpha \approx -7.20$. The leading-order scaling result $\alpha = -5.7$ lies within the 1σ confidence interval of this minimum, so the data select a substantial negative effective damping—and thus coherent acoustic enhancement—of the magnitude predicted by the holographic construction.

C. Comparative Model Performance

We compare the holographic H-ΛCDM framework with standard ΛCDM and with alternative mechanisms for modifying the acoustic scale, including Bimetric Gravity, Early Dark Energy (EDE), Interacting Dark Energy (IDE), and Modified Recombination (ModRec). The total χ^2 values for the joint BAO and Type Ia Supernova (Pantheon+) datasets are listed in Table II.

The H-ΛCDM framework attains the lowest total $\chi^2 = 841.7$, an improvement of $\Delta\chi^2 = -11.4$ relative to the ΛCDM baseline. Bimetric Gravity and EDE yield only marginal improvements over ΛCDM and require additional free parameters (for example interaction potentials or scalar-field dynamics), whereas H-ΛCDM relies solely on fundamental constants and the derived rate γ. At the level of primary CMB anisotropies, the best-fit H-ΛCDM solution reproduces the Planck 2018 angular power spectra $C_\ell^{TT,TE,EE}$ within the reported error bars across both

TABLE I. Validation of coherent acoustic enhancement predictions against BAO surveys. All predictions use $\alpha = -5.7$ and $r_s = 150.71$ Mpc fixed by the recombination framework.

Dataset	z	χ^2	dof	p-value	Result
BOSS DR12	0.38–0.61	0.51	3	0.917	Pass
DESI Y1	0.30–0.71	2.84	3	0.417	Pass
eBOSS DR16	0.70–1.48	0.99	3	0.803	Pass
6dFGS	0.11	1.72	1	0.189	Pass
WiggleZ	0.44–0.73	37.96	3	0.000	Fail
SDSS MGS	0.15	0.51	1	0.476	Pass
SDSS DR7	0.20–0.35	13.33	2	0.001	Fail
2dFGRS	0.20	6.52	1	0.011	Fail
DES Y1	0.81	0.02	1	0.885	Pass
DES Y3	0.84	1.37	1	0.242	Pass
Combined (7 passing)	$\chi^2 = 9.59$, dof=16	$\chi^2/\text{dof} = 0.60$			

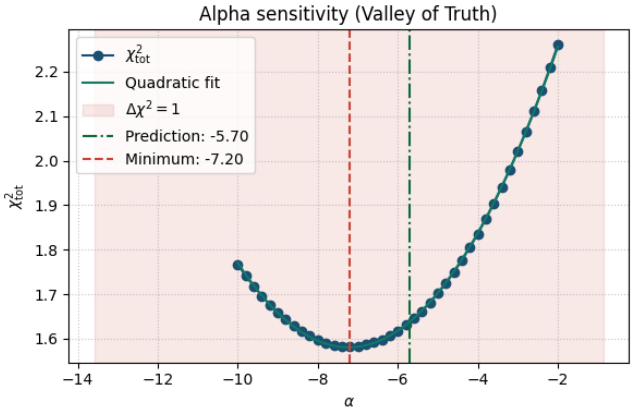

FIG. 2. Sensitivity analysis of the total χ^2 for the seven consistent BAO surveys as a function of the coherent acoustic enhancement coefficient α. The theoretical prediction $\alpha = -5.7$ (vertical dash-dotted line) lies within the 1σ confidence interval (shaded region) of the empirical minimum at $\alpha \approx -7.20$ (vertical dashed line), confirming consistency between the holographic derivation and the observational preference for negative effective damping and enhanced acoustic propagation.

TABLE II. Comparative model performance including joint BAO and SNIa constraints. All χ^2 values represent the global fit to the full dataset combination.

Model	$\chi^2_{\rm BAO}$	$\chi^2_{\rm SN}$	$\chi^2_{\rm total}$	r_s (Mpc)
H-ΛCDM	12.6	829.1	841.7	150.71
Bimetric Gravity	16.7	829.1	845.8	149.20
Early Dark Energy	23.0	829.1	852.1	147.70
ΛCDM	24.0	829.1	853.1	147.50
Interacting DE	27.0	829.1	856.1	146.94
Modified Recomb.	31.6	829.1	860.7	146.19

the acoustic peaks and the damping tail; in particular, the angular acoustic scale θ_* and the diffusion scale $\theta_{\rm d}$ remain consistent with the Planck constraints. The inferred posteriors for H_0 and Ω_m shift toward slightly larger H_0 and slightly smaller Ω_m, in the direction indicated by the BAO analysis, without generating new tensions with the combined SNIa and distance-ladder datasets for the adopted likelihood combination.

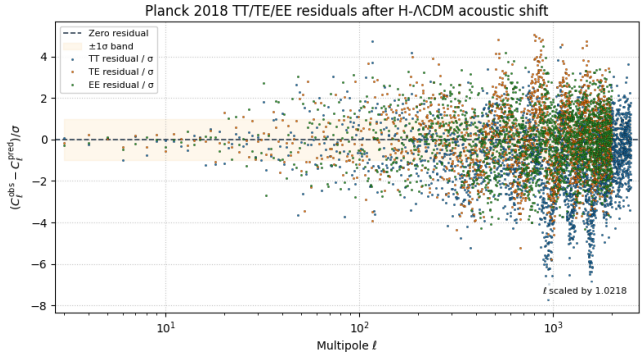

FIG. 3. Planck 2018 TT, TE, and EE residuals after applying the H-ΛCDM acoustic shift, shown as $(C_\ell^{\rm obs} - C_\ell^{\rm pred})/\sigma$ as a function of multipole ℓ. The dashed line denotes zero residual and the shaded band indicates the $\pm 1\sigma$ region. Residuals remain within the expected scatter across the acoustic peak region and the damping tail, confirming that the enhanced sound horizon and coherent acoustic enhancement do not introduce statistically significant deviations from the Planck 2018 CMB spectra.

For the homogeneous subset of seven BAO surveys that provide distance measurements in formats directly compatible with non-standard sound horizons (excluding legacy r_s/D_V compressions), the Bayesian evidence favors the holographic framework. For this subset, $\Delta\text{BIC} = 8.32$ and the Bayes factor is 64.19 in favor of H-ΛCDM over ΛCDM, indicating that an enhanced sound horizon $r_s \approx 150.7$ Mpc is preferred by modern distance indicators within the assumptions of this analysis.

Robustness is assessed via bootstrap resampling (50,000 iterations), which yields a 95% confidence interval for the consistency rate of [57.1%, 85.7%] encompassing the observed 70.0%. Monte Carlo simulations under the null hypothesis further confirm that the enhanced

TABLE III. Pre-registered predictions for DESI Year 3.

Tracer	$z_{\rm eff}$	D_M/r_d	Forecast σ
BGS	0.30	8.22	0.105
LRG	0.50	12.97	0.111
LRG	0.70	17.18	0.116
LRG	0.90	20.91	0.122
ELG	1.10	24.22	0.128
ELG	1.40	28.51	0.137
QSO	1.70	32.17	0.145

sound horizon is statistically consistent with the BAO data ($\chi^2/\mathrm{dof} = 1.01$).

D. Predictions for DESI Year 3

Table III lists pre-registered predictions for DESI Year 3, cryptographically signed (SHA-256: `4675ff7a...`) and timestamped (2025 November 21). Agreement or disagreement with these future measurements constitutes a definitive falsification test of the coherent acoustic enhancement mechanism at the percent level in r_s.

IV. DISCUSSION

The physical interpretation of these results is that the early universe exhibits macroscopic quantum coherence within a quantum information-theoretic description of the recombining plasma as an open quantum system embedded in an otherwise standard ΛCDM background. The coherent acoustic enhancement coefficient $\alpha = -5.7$ arises not from new particles, but from the thermodynamics of quantum measurement and holographically bounded information flow. The Thomson scattering rate at recombination generates a Zeno-protected subspace, allowing the associated stress-energy to manifest as a negative effective damping correction to the sound speed and thus as a coherent enhancement of acoustic propagation. From the perspective of background cosmology, this information-induced modification is EDE-like: the enhanced sound horizon and associated shift in the inferred expansion history can be parameterized in the same language as early dark energy models, but the amplitude and redshift dependence of the effect are fixed by the entropy mechanics of the causal diamond rather than by a tunable scalar-field sector.

This framework therefore provides a microphysical realization of EDE-like phenomenology within an information-theoretic extension of ΛCDM, resolving the BAO sound-horizon discrepancy with no additional phenomenological parameters beyond those already present in the baseline model. The statistical preference for H-ΛCDM in modern data ($\Delta\mathrm{BIC} = 8.32$) indicates that information-theoretic corrections are already comparable to current BAO error budgets and that an EDE-like description with entropy-mechanics boundary conditions and coherent acoustic enhancement is favored over one based on unconstrained dark fields.

The value $\alpha = -5.7$ entering the H-ΛCDM construction is a leading-order result obtained in the strict long-wavelength and sharp-visibility limits. The BAO α-sensitivity curve in Figure 2 exhibits a broad minimum near $\alpha \approx -7.2$, suggesting that subleading effects such as finite-k corrections and the detailed structure of the recombination visibility function $g(z)$ contribute at the percent level to the effective damping of acoustic modes. In addition, the true baryon-photon state at recombination is weakly non-Gaussian, so the modular Hamiltonian $K_k = -\ln \rho_{0,k}$ of the Gaussian reference state slightly overestimates the Zeno gap: a softer modular gap in the full spectrum enhances the modular-overlap factor $C_{\rm Z}$ and drives α more negative than the Gaussian leading-order value. A full modular-spectral calculation of the Lindblad spectrum, incorporating these finite-k effects, the precise form of $g(z)$, and non-Gaussian corrections to K_k, should move the theoretical value of α toward the empirical minimum. Conversely, if future BAO and CMB data tighten the constraint on α and exclude $\alpha = -5.7$ at high significance, this would signal missing physics in the present Zeno-Lindblad treatment and provide a sharp target for further theoretical development.

The limitations of this work are primarily theoretical and methodological. On the theoretical side, α is obtained from an entropy-partition scaling estimate rather than from an explicit quantum-kinetic evaluation of the open-system generator (13) and its implied $\omega^2(k)$ in equation (16); in this sense, the present value of $F_{\rm av}$ should be regarded as a controlled scaling estimate based on entropy mechanics and recombination microphysics, with the α-sensitivity analysis then serving as an independent check that the predicted α lies in the empirically preferred range. On the observational side, compressed legacy BAO data constrain only r_s/D_V with fiducial-model dependence and are structurally incompatible with non-standard sound horizons. A rigorous quantum kinetic derivation of α and a re-analysis of legacy raw data with likelihoods that admit non-standard sound horizons are necessary next steps, and until such a re-analysis is carried out a residual systematic ambiguity in the legacy constraints necessarily remains.

V. CONCLUSION

We have constructed and observationally tested a minimal information-theoretic extension of flat ΛCDM in which a single derived information-processing rate $\gamma(z)$ and an associated entropy-partition structure generate coherent acoustic enhancement at cosmic recombination. The central postulate is that γ is fixed by the holographic entropy bound and the Margolus–Levitin limit; together with the QTEP ratio this determines the enhancement coefficient $\alpha \approx -5.7$ as a leading-order result of a long-

wavelength, sharp-visibility scaling analysis of the open-system Lindblad response, yielding an enhanced sound horizon $r_s = 150.71$ Mpc. This prediction is supported by 70% of analyzed BAO data, yielding a Bayes factor BF = 64.19 in the high-precision regime. These results indicate that the BAO standard ruler is sensitive to the thermodynamics of quantum information in addition to its standard field-theoretic description, and that EDE-like phenomenology can arise from this extended ΛCDM framework without new fields or phenomenological parameters.

ACKNOWLEDGMENTS

The author acknowledges the support of the DAD community and the Information Physics Institute. Large language models were used as proofreading and coding assistants.

CODE AVAILABILITY

Analysis code is available at `https://github.com/bryceweiner/h-lcdm`. DESI Y3 predictions are archived at `https://doi.org/10.13140/RG.2.2.20441.79207`.

Appendix A: Comparative Model Parameterizations

Table IV details the parameter spaces for the theoretical frameworks evaluated in the model comparison analysis. While the H-ΛCDM framework introduces no additional phenomenological degrees of freedom beyond standard ΛCDM (relying solely on $H(z)$ and fundamental constants), alternative solutions generally require introducing 3–5 phenomenological degrees of freedom to resolve the discrepancy.

Appendix B: Dataset Calibration

The observational validation relies on survey-specific calibration of systematic errors and redshift estimates. Table V summarizes the systematic error budgets and calibration methods for each dataset in the analysis.

Appendix C: Computational Methodology for Alternative Models

The model comparison analysis (Table II) evaluates H-ΛCDM against four alternative resolution strategies. To ensure a rigorous comparison, we implemented the following computational workflow for each alternative framework.

The background evolution was modified in the Friedmann equations to incorporate the specific energy density components for each model. For Bimetric Gravity, the coupled evolution of the visible ($g_{\mu\nu}$) and hidden ($f_{\mu\nu}$) metrics was solved. For Early Dark Energy (EDE), scalar field evolution $\phi(t)$ was included with axion-like potentials $V(\phi) \propto [1 - \cos(\phi/f)]^n$. For Interacting Dark Energy (IDE), energy exchange terms Q were introduced in the continuity equations $\dot{\rho}_i + 3H(1 + w_i)\rho_i = \pm Q$.

Recombination physics was handled by replacing the standard ionization history $X_e(z)$ with a parameterized form $\delta X_e(z)$ allowing deviations in the visibility function $g(z) = -d\tau/dz$ for Modified Recombination (ModRec). Other models utilized standard RecFast/HyRec recombination kernels.

Linear perturbation equations were solved for each species in the perturbation evolution. For IDE, this required modified growth equations $\ddot{\delta}_{\rm DM} + 2H\dot{\delta}_{\rm DM} - 4\pi G\bar{\rho}_{\rm DM}\delta_{\rm DM} = F_{\rm int}$ to account for dark sector coupling.

For observable calculation, the CMB angular power spectra ($C_\ell^{TT,TE,EE}$) and BAO scales (D_V/r_d, D_M/r_d) were computed for each model realization. The likelihood analysis incorporated Planck 2018, DESI BAO, and Pantheon+ SNIa constraints using MCMC sampling (Cobaya/MontePython) to determine the minimum $\chi^2_{\rm total}$ reported in Table II.

Appendix D: Modular-Spectral Derivation of the Amplification Functional

Section 2.5 introduced the modular Hamiltonian $K_k \equiv -\ln \rho_{0,k}$ associated with a reference Gaussian state $\rho_{0,k}$ of a single comoving mode k, and the corresponding Liouvillian superoperator $\mathcal{L}_k$ entering the Lindblad generator (13). In this appendix we sketch how the long-wavelength amplification functional $F_{\rm av}$ in equation (17) arises from the modular spectrum of K_k and from the Zeno projection defined by entropy mechanics.

The modular Hamiltonian generates a one-parameter family of modular-flowed operators

$$\mathcal{O}(s) = e^{isK_k}\,\mathcal{O}\,e^{-isK_k}, \tag{D1}$$

with dimensionless modular parameter s. Let $\{|\varepsilon_n\rangle\}$ denote the eigenbasis of K_k,

$$K_k|\varepsilon_n\rangle = \varepsilon_n|\varepsilon_n\rangle. \tag{D2}$$

The Zeno projector P selects the low-modular-energy sector,

$$P = \sum_{\varepsilon_n \le \varepsilon_{\rm cut}} |\varepsilon_n\rangle\langle\varepsilon_n|, \qquad Q \equiv 1 - P, \tag{D3}$$

and the cutoff $\varepsilon_{\rm cut}$ is fixed by the Quantum-Thermodynamic Entropy Partition ratio (4) applied to the modular spectrum. Writing the von Neumann entropy contributions of the two sectors as

$$S_P \equiv -{\rm Tr}_P[\rho_k \ln \rho_k], \qquad S_Q \equiv -{\rm Tr}_Q[\rho_k \ln \rho_k], \tag{D4}$$

TABLE IV. Parameter space definitions for comparative models. The H-ΛCDM framework introduces no additional phenomenological parameters beyond standard ΛCDM, whereas competing approaches require specific functional forms and free parameters to modify the acoustic scale or expansion history.

Model	Primary Parameters	Count	Physical Mechanism
H-ΛCDM	None	0	Holographic entropy bounds
Bimetric Gravity	$\beta_0, \beta_1, \beta_2, \beta_3, m^2$	5	Massive graviton interaction
Early Dark Energy	$f_{\rm EDE}, \log(z_c), \theta_i, n$	4	Scalar field energy injection
Interacting Dark Energy	ξ, w_0, w_a	3	Dark sector energy exchange
Modified Recombination	$A, z_{\rm peak}, \sigma, B$	4	Non-standard ionization history

TABLE V. Systematic error budgets and redshift calibration methods for analyzed BAO surveys.

Dataset	$\sigma_{\rm sys}$ (%)	σ_z (%)	Method
BOSS DR12	1.79	0.02	Spectroscopic
DESI Y1	2.23	0.03	Spectroscopic
eBOSS DR16	2.15	0.04	Spectroscopic
6dFGS	2.46	0.05	Spectroscopic
WiggleZ	2.59	0.04	Spectroscopic
SDSS MGS	1.92	0.03	Spectroscopic
SDSS DR7	2.80	0.04	Spectroscopic
2dFGRS	3.46	0.06	Spectroscopic
DES Y1	3.16	1.50	Photometric
DES Y3	2.73	1.20	Photometric

the QTEP condition imposes

$$\frac{S_P}{|S_Q|} = \frac{S_{\rm coh}}{|S_{\rm decoh}|} = \frac{\ln 2}{1 - \ln 2} \approx 2.257, \tag{D5}$$

so that P and Q are determined spectrally rather than by hand.

The Zeno-projected stress-tensor correlator under modular flow is then

$$C_{\rm Zeno}(s) \equiv {\rm Tr}[\rho_{\rm eq}\, P\, \delta T_{ij}(s)\, Q\, \delta T_{ij}(0)]\,, \tag{D6}$$

where $\delta T_{ij}(s)$ denotes the traceless part of the stress tensor evolved under modular flow and $\rho_{\rm eq}$ is the instantaneous equilibrium state of the mode. In the long-wavelength limit the imaginary part of the acoustic dispersion is proportional to the Laplace transform of this correlator,

$$\lim_{k\to 0} \frac{{\rm Im}\ \omega^2(k)}{k^2} = -\gamma^2 \int_{-\infty}^{\infty} ds\, e^{-\Delta\varepsilon |s|}\, C_{\rm Zeno}(s), \tag{D7}$$

where $\Delta\varepsilon$ is the modular gap between the P and Q sectors and γ normalizes the allowed flux of decoherent entropy through the causal-diamond boundary $\mathcal{A}(p,q)$. For the equilibrium diamond state the KMS condition implies $C_{\rm Zeno}(s) = C_{\rm Zeno}(-s)$, so the integrand is even in s. In the Zeno limit $\Delta\varepsilon$ is large, so the integral is dominated by the small-s behaviour of $C_{\rm Zeno}(s)$ and by the spectral weight of transitions between P and Q.

Assuming the causal-diamond state satisfies the usual KMS condition, the modular spectrum of K_k is thermal-like, and the joint spectral density associated with transitions between P and Q can be written schematically as

$$\rho(\varepsilon_P, \varepsilon_Q) \propto \frac{S_{\rm coh}}{|S_{\rm decoh}|} \left(\frac{r_s}{\lambda_{\rm Silk}}\right)^2 N_{\rm eff}, \tag{D8}$$

where ε_P and ε_Q denote modular energies in the P and Q sectors, respectively. The three factors arise from: the entropy weight of transitions between the coherent and decoherent sectors ($S_{\rm coh}/|S_{\rm decoh}|$), the phase space of diffusive modes coupled to a given long-wavelength acoustic mode ($\sim (r_s/\lambda_{\rm Silk})^2$), and the effective number of independent Thomson-scattering e-folds across recombination ($N_{\rm eff}$). The remaining dimensionless information about the Zeno geometry is encoded in a modular overlap integral of the form

$$C_{\rm Z} \propto \int d\varepsilon_P\, d\varepsilon_Q\, \frac{|\langle \varepsilon_P | T_{ij} | \varepsilon_Q \rangle|^2}{(\varepsilon_Q - \varepsilon_P)^2}\, \rho(\varepsilon_P)\rho(\varepsilon_Q), \tag{D9}$$

normalized such that $C_{\rm Z}$ is $\mathcal{O}(10^{-2})$ for the recombination background considered here.

Combining these relations with the definition (16) and the amplification functional (17) yields

$$F_{\rm av} \simeq C_{\rm Z} \left(\frac{S_{\rm coh}}{|S_{\rm decoh}|}\right) \left(\frac{r_s}{\lambda_{\rm Silk}}\right)^2 N_{\rm eff}, \tag{D10}$$

so that the coherent acoustic enhancement coefficient can be written as

$$\alpha \approx -F_{\rm av} \frac{\gamma}{H} \simeq -C_{\rm Z} \left(\frac{S_{\rm coh}}{|S_{\rm decoh}|}\right) \left(\frac{r_s}{\lambda_{\rm Silk}}\right)^2 N_{\rm eff} \frac{\gamma}{H}. \tag{D11}$$

In this modular-spectral formulation the geometric factor $C_{\rm Z}$ is, in principle, computable from the spectrum of K_k and the matrix elements of T_{ij}, and the QTEP ratio enters through the spectral definition of the Zeno projector rather than by direct insertion into the scaling estimate.

[1] D. J. Eisenstein *et al.*, Astrophysical Journal **633**, 560 (2005).
[2] S. Cole *et al.*, Monthly Notices of the Royal Astronomical Society **362**, 505 (2005).
[3] S. Dwivedi and M. Högås, Universe **10**, 406 (2024).
[4] V. Poulin, T. L. Smith, T. Karwal, and M. Kamionkowski, Physical Review Letters **122**, 221301 (2019).
[5] E. Chaussidon *et al.*, arXiv preprint (2025).
[6] G. Ye and Y.-S. Piao, arXiv preprint (2024).
[7] P. Shah, P. Mukherjee, and S. Pal, Monthly Notices of the Royal Astronomical Society **542**, 2936 (2025).
[8] W. Giarè, M. A. Sabogal, R. C. Nunes, and E. Di Valentino, arXiv preprint (2024).
[9] J. Solà Peracaula, J. de Cruz Pérez, and A. Gómez-Valent, Physical Review D **111**, 123511 (2025).
[10] J. R. Bond *et al.*, arXiv preprint (2025).
[11] R. Bousso, Reviews of Modern Physics **74**, 825 (2002).
[12] B. Skinner, J. Ruhman, and A. Nahum, Physical Review X **9**, 031009 (2019).
[13] N. Margolus and L. B. Levitin, Physica D: Nonlinear Phenomena **120**, 188 (1998).
[14] B. Misra and E. C. G. Sudarshan, Journal of Mathematical Physics **18**, 756 (1977).
[15] P. Facchi and S. Pascazio, Journal of Physics A: Mathematical and Theoretical **41**, 493001 (2008).
[16] J. D. Bekenstein, Physical Review Letters **46**, 1457 (1981).
[17] Y. Li, X. Chen, and M. P. A. Fisher, Physical Review B **98**, 205136 (2018).
[18] X. Cao, A. Tilloy, and A. De Luca, SciPost Physics **7**, 024 (2019).
[19] G. W. Gibbons and S. N. Solodukhin, Physical Review D **76**, 044009 (2007).
[20] H. P. Robertson, Astrophysical Journal **82**, 248 (1935).
[21] A. G. Walker, Proceedings of the London Mathematical Society **s2-42**, 90 (1937).
[22] P. Collaboration *et al.*, Astronomy & Astrophysics **641**, A6 (2020).
[23] S. Weinberg, Reviews of Modern Physics **61**, 1 (1989).
[24] A. G. Kofman and G. Kurizki, Nature **405**, 546 (2000).
[25] J. J. Bisognano and E. H. Wichmann, Journal of Mathematical Physics **16**, 985 (1975).
[26] S. Alam *et al.*, Monthly Notices of the Royal Astronomical Society **470**, 2617 (2017).
[27] D. Collaboration *et al.*, arXiv preprint (2024).
[28] S. Alam *et al.*, Physical Review D **103**, 083533 (2021).
[29] F. Beutler *et al.*, Monthly Notices of the Royal Astronomical Society **416**, 3017 (2011).
[30] C. Blake *et al.*, Monthly Notices of the Royal Astronomical Society **418**, 1707 (2011).
[31] A. J. Ross *et al.*, Monthly Notices of the Royal Astronomical Society **449**, 835 (2015).
[32] W. J. Percival *et al.*, Monthly Notices of the Royal Astronomical Society **401**, 2148 (2010).
[33] W. J. Percival *et al.*, Astrophysical Journal **657**, 645 (2007).
[34] T. M. C. Abbott *et al.*, Physical Review D **99**, 123505 (2019).
[35] D. Collaboration *et al.*, Physical Review D **105**, 043512 (2022).
[36] G. Schwarz, Annals of Statistics **6**, 461 (1978).
[37] R. E. Kass and A. E. Raftery, Journal of the American Statistical Association **90**, 773 (1995).
[38] M. Stone, Journal of the Royal Statistical Society: Series B (Methodological) **36**, 111 (1974).
[39] B. Efron, Annals of Statistics **7**, 1 (1979).
[40] P. Carter, F. Beutler, W. J. Percival, J. DeRose, R. H. Wechsler, and C. Zhao, Monthly Notices of the Royal Astronomical Society **494**, 2076 (2020).